PAPER

Probing the binding behavior and kinetics of silver nanoparticles with bovine serum albumin†

Gongke Wang,‡*a Yanfang Lu,‡a Huimin Hou‡a and Yufang Liu‡*b

Nanomaterials have been utilized as multifunctional diagnostic and therapeutic agents. However, the effective application of nanomaterials is hampered by our limited understanding and control over their interactions with specific biological systems. Elucidating the binding mechanism and kinetic behavior of metal nanomaterials with proteins is significant, and herein we investigate the interaction of a model protein, bovine serum albumin (BSA), with silver nanoparticles (AgNPs) using fluorescence, synchronous fluorescence, ultraviolet (UV) absorption, Fourier transform infrared spectroscopy (FT-IR) and circular dichroism (CD) techniques in aqueous solutions. The experimental results indicated that the binding of AgNPs to BSA seems to be of a static quenching type with the formation of a ground state complex. With the determination of the binding constants and thermodynamic parameters, it is suggested that the binding process of AgNPs to the surface of BSA is spontaneous. Moreover, it was demonstrated that the main acting forces between the AgNPs and BSA may be hydrophobic and electrostatic interactions. At the same time, synchronous fluorescence, FT-IR and CD techniques were employed to analyze the conformational change of BSA in the presence of AgNPs. The results of kinetic studies reveal that the adsorption of BSA on the AgNP surface tends to have pseudo-second-order kinetic characteristics with an obvious hysteresis effect.

1. Introduction

As one of the most common nanomaterials, silver nanoparticles (AgNPs) have been paid a lot of attention with their unique properties including small-scale effects, optical effects, antimicrobial activity, excellent stability and biocompatibility.[1,2] Due to their superior performance, AgNPs have been widely used in biosensing, chemical catalysis, and solar energy harvesting,[2–4] especially in the field of life science research. Therefore, it is not hard to notice that there will be great potential in studying the interactions between AgNPs and proteins, which could facilitate the understanding of biological effects and safe application of AgNPs in biological systems.[2,5–7]

Recent research has revealed that once AgNPs enter a physiological environment, they can be readily coated with proteins, lipids, and other biomolecules. When proteins cover the surface of the AgNPs, forming what is known as a biocorona, this decides the fate of the AgNPs *in vivo*.[8–11] Sharma and coworkers reviewed the effects of the coating on AgNPs on the fate, stability and toxicity of the AgNPs in aqueous solutions and biological systems.[12] It was shown that the key factors contributing to the fate and toxicity of AgNPs are the size, shape, surface coating, surface charge and conditions of silver ion release, which provide some new insight into understanding the biological impact of AgNPs on humans and organisms. Consequently, this has led to increased interest in acquiring information on protein/AgNP interactions and the biological implications of these interactions. Spectroscopic studies on the interaction between specific ligand-stabilized AgNPs with different proteins confirmed the formation of a typical protein corona and offered a possible binding mechanism.[13–15] Zhang *et al.* investigated the effects of cysteine residues on protein interactions with AgNPs, and found that the protein cysteine content has no effect on the kinetics of the protein/AgNP binding, whereas proteins that contain reduced cysteine residues can induce significant AgNP dissolution.[16] At the same time, detailed kinetic, thermodynamic and structural studies on a HSA-AgNP system gave a reasonable explanation of the action forces and arrangement of HSA binding to the AgNP surface.[17] Moreover, the binding of serum albumins to AgNPs further demonstrated the palpable hysteresis effect that accompanies the aggregation of AgNPs and the conformational changes of the protein.[18] Besides the studies on the binding mechanism and kinetics of AgNPs with

aSchool of Chemistry and Chemical Engineering, Key Laboratory of Green Chemical Media and Reactions, Ministry of Education, Collaborative Innovation Center of Henan Province for Green Manufacturing of Fine Chemicals, Henan Normal University, Xinxiang, Henan 453007, P. R. China. E-mail: wanggongke@126.com; yf-liu@htu.cn; Fax: +86-373-3325249; Tel: +86-373-3325249

bSchool of Physics and Materials Science, Henan Normal University, Xinxiang, Henan 453007, P. R. China

† Electronic supplementary information (ESI) available. See DOI: 10.1039/c6ra26089f

‡ Postal address: School of Chemistry and Chemical Engineering, Henan Normal University, 46 Jian-she Road, Mu Ye District, Xinxiang 453007, PR China.

proteins, the thermostability of the AgNP/protein systems has been paid significant attention in recent years. This is because one of the properties of AgNPs which is crucial for all their applications is their stability. Tsai's group found that surface conjugation with BSA can effectively prevent AgNPs from aggregating in an acidic environment, and both the aggregation rate constant and the extent of aggregation of AgNPs seem to be correlated with the properties of the protein corona on the AgNPs.[10] Ding and coworkers examined the thermostability and reversibility of AgNP–lysozyme (alpha lactalbumin) interactions using spectroscopic and discrete molecular dynamics (DMD) simulation techniques, and evaluated the effects of different capping agents of AgNPs on the structure, dynamics and thermodynamics of the protein-AgNP complex, thus providing an effective strategy for facilitating our comprehension of the biological implications of engineered nanomaterials.[19] As a highlighted development, Atreya unraveled a mechanism through which silver nanoparticles are rendered ultrastable in an aqueous solution when complexed with the protein ubiquitin, which involves the dynamic and reversible association and dissociation of ubiquitin from the surface of the AgNPs. This study provides new insights into the mechanisms of protein–AgNP interactions and opens up new avenues for their application in a wide range of systems.[20]

However, unlike gold, the susceptibility of silver to oxidation has restricted the development of important silver-based nanomaterials. Therefore, research on the interactions of AgNPs with proteins is flourishing, but is still limited, and more and more other nanomaterials are being brought to our attention, such as gold nanoparticles (AuNPs). Owing to their more excellent biocompatibility and stability, the interaction of AuNPs with proteins has been a hotspot of current research.[21–25] In this context, so far interaction information for the binding of serum albumins to AgNPs, such as the binding properties, the kinetic behavior and the conformational changes of the proteins, has been rarely explored. It is obvious that elucidating these fundamental issues will be helpful for providing important information on the biological effects of AgNPs in organisms, and for promoting the effective and safe application of AgNPs in biological and medical areas.

Herein, we studied the interaction of AgNPs with BSA in aqueous solutions, and analyzed the binding mechanism and kinetic behavior in detail. The specific binding properties, the adsorption kinetic behavior and protein conformational changes in the binding process were investigated systematically using multiple techniques. We believe that comprehensive understanding of the AgNP-protein interaction will be beneficial to further develop functionalized and safe AgNPs in the future.

2. Experimental

2.1. Materials and methods

Silver nitrate was obtained from TianDa Chemical Reagent Co., Ltd (Tianjin, China). Trisodium citrate was purchased from Alfa-Aesar (USA). Bovine Serum Albumin (BSA, MW 66 kDa) was procured from Sigma-Aldrich Chemical Company (USA). A 1.0

$\times 10^{-4}$ M BSA stock solution was prepared by dissolving BSA in 10 mL of 0.01 M phosphate buffer solution (PBS, pH 7.4). The pH values of the solutions were measured using a pHS-2C pH-meter (Shanghai Dapu Instruments Co., Ltd, Shanghai, China) at room temperature. Ultrapure water was used throughout the experimental process. All of the stock solutions were kept in a refrigerator at 0–4 °C.

2.2. Preparation of AgNPs

All glassware used in the experiment was cleaned in a bath of freshly prepared aqua regia and rinsed thoroughly in ultrapure water prior to use. The AgNPs were prepared following Munro's method.[26] In our case, 100 mL of ultrapure water was heated to 45 °C, then some solid silver nitrate was added. When the aqueous solution was heated to boiling, 2 mL of trisodium citrate (1%) was added. The boiling solution was stirred for another 30 min and then stored as the stock solution. In order to avoid the oxidation and aggregation of the AgNPs, the stock solution of the AgNPs was sealed in a refrigerator at 4 °C and used within 4 days. The size and morphology of the AgNPs were characterized using a TU-1810 spectrophotometer (Puxi Analytic Instrument Ltd., China) equipped with 1.0 cm quartz cells, a TEM (transmission electron microscope, JEM 2100) and XRD (X-ray diffraction, D8 Advance).

2.3. Fluorescence measurements

Fluorescence measurements were performed on a CARY Eclipse fluorescence spectrophotometer (Varian, America). The spectra were recorded in the wavelength range of 290–500 nm upon excitation at 280 nm, using 5 nm/5 nm slit widths, and each spectrum was the average of three scans. The fluorescence emission of BSA (100 μL) was obtained in the absence and presence of AgNPs, and the final concentration of AgNPs reached 1.0×10^{-10} M. In order to study the effect of temperature on the binding of BSA to the AgNPs, the fluorescence emission was evaluated at different temperatures (298, 303 and 310 K). The temperature was controlled with a SHP-0515 thermostatic waterbath.

2.4. Synchronous fluorescence studies

It is known that synchronous fluorescence spectra can offer characteristic information on tyrosine and tryptophan residues. When the wavelength difference $\Delta\lambda = \lambda_{em} - \lambda_{ex}$ was fixed at either 15 or 60 nm, the synchronous fluorescence spectra of BSA were measured and used to estimate the conformational changes of the protein.

2.5. FT-IR measurements

FT-IR measurements were performed with a type of 360 ESP FT-IR spectrometer (Perkin Elmer). All spectra were collected using the ATR method with a resolution of 4 cm^{-1}. The FT-IR spectra of BSA, in the absence and presence of AgNPs, were recorded in the range of 1700–1500 cm^{-1} in PBS (pH 7.4) and at room temperature. The secondary structure changes of BSA and the

BSA/AgNP complexes were evaluated from the variation of the amide I band, located at 1650–1660 cm^{-1}.

2.6. Circular Dichroism (CD) measurements

The CD spectra measurements were carried out on a Chirascan spectropolarimeter (Applied Photophysics Ltd., England) under a constant nitrogen flush. A quartz cell with a path length of 1.0 cm was used in the range of 190–260 nm at room temperature. Three scans were accumulated with a continuous scan mode. The bandwidth was 1.0 nm and the scan speed was 10 nm min^{-1} with a response time of 2 s. The final concentration of BSA was 1×10^{-6} M, and the AgNP concentrations were 0, 2.0×10^{-11} M, 6.0×10^{-11} M and 2.0×10^{-10} M, in phosphate buffer (PBS, 0.01 M, pH 7.40). All observed CD spectra were baseline subtracted for air, and the results were taken as CD ellipticity in mdeg.

3. Results and discussion

3.1. Characterization of the synthesized AgNPs

The absorption spectra of the AgNPs freshly prepared and after centrifugal processing were recorded at room temperature (Fig. S1†). From the intensity and position of the surface plasmon absorption peak of the nanoparticles (NPs), we can ascertain the size and dispersity of the NPs. As shown in Fig. S1A,† the surface plasmon band of the AgNPs exhibits a maximum at about 421 nm, which is in good accordance with previous reports.[27] Fig. S1B† is the absorption spectrum after centrifugal processing. It can be seen that the maximum absorption of the AgNPs has a blue shift of about 5 nm. Moreover, it is found that the absorption peak of citrate (210 nm) seems to have disappeared. These observations illustrate that citrate on the surface of the AgNPs may be detached, which may lead to the slight aggregation of AgNPs to a certain degree. Additionally, it is found that the synthesized AgNPs have good monodispersity according to the symmetrical shape of the peak. The morphology and structure of the AgNPs were observed using a TEM (Fig. S2†). We can see that the prepared spherical AgNPs are monodispersed, and the average size is determined as 40 ± 5 nm from the TEM micrograph. XRD analysis illustrated three distinct diffraction peaks at 38.1°, 44.1° and 64.1°, which correspond to the planes {111}, {200} and {220} of cubic face-centered silver (shown in Fig. S3†). The lattice constant in this work was $a = 4.086$ Å, which matches the data in the database of the Joint Committee on Powder Diffraction Standards (JCPDS), file no. 04-0783.[28] The average size of the AgNPs formed in the bioreduction process was determined as 35 nm using Scherrer's equation.[28] Consequently, the results of the XRD pattern are in agreement with those of the TEM micrograph.

3.2. Mechanism of fluorescence quenching and binding mode

Fluorescence quenching that refers to any process that decreases the fluorescence intensity of a sample is usually a result of different types of molecular interactions, including excited state reactions, energy transfer, molecular rearrangements, the formation of ground state complexes and collisional diffusion. Quenching can be induced by different mechanisms, which are usually classified into dynamic quenching and static quenching. Dynamic collisional quenching occurs when an excited state fluorophore is deactivated upon contact with a quencher molecule in solution. In this case the fluorophore is returned to the ground state during a diffusive encounter with the quencher. Static quenching occurs due to the formation of a ground state complex between the fluorophore and the quencher. Dynamic and static quenching can be distinguished by their differing dependence on temperature. Higher temperatures result in faster diffusion and larger amounts of collisional quenching, and will typically lead to the dissociation of weakly bound complexes. Consequently, the quenching constant usually increases with an increase in the temperature for dynamic quenching. However, for the static quenching mode, the quenching constant will decrease at higher temperatures.[29,30]

In our case, the concentration of BSA was constant at 1.0 μM, and the AgNPs were added to a maximal concentration (10^{-10} M). Fig. 1A shows the fluorescence emission spectra of BSA in the absence and presence of AgNPs upon excitation at 298 K. It can be observed that as the concentration of AgNPs increases the emission intensity of BSA decreases gradually with a blue shift of around 5–6 nm, indicating that the AgNPs can effectively quench the intrinsic fluorescence of BSA. Additionally, the blue shift of the fluorescence emission seems to originate from the changes in BSA conformation. For quantitative analysis of the quenching mechanism of AgNPs with BSA, the fluorescence quenching process was studied using the following equation:[29]

$$\frac{F_0}{F} = 1 + k_q \tau_0 [Q] = 1 + K_{SV}[Q] \tag{1}$$

where F_0 and F represent the fluorescence of the protein in the absence and presence of the quencher (AgNPs), k_q and K_{SV} are the bimolecular quenching rate constant and Stern–Volmer quenching constant, respectively, τ_0 represents the average lifetime of the biomolecule, and $[Q]$ is the quencher concentration.

Fig. 1B shows F_0/F as a function of $[Q]$, and Table 1 lists the Stern–Volmer quenching constants K_{SV} and quenching rate constants k_q at different temperatures. From Table 1, it is seen that the quenching constant K_{SV} is inversely correlated with the temperature, which demonstrates that the fluorescence quenching is probably due to the formation of the ground state complex between the AgNPs and BSA. Furthermore, we can find that the quenching rate constants k_q determined here are significantly greater than the value of 2.0×10^{10} M^{-1} s^{-1} that is usually regarded as the maximal diffusion constant of biomolecules. The combination of these observations seems to suggest that the binding of BSA to AgNPs may be of the static quenching type.[31]

As for a static quenching process, the AgNP/BSA complex can be analyzed using the following equation:[32]

$$\log \frac{F_0 - F}{F} = \log K_b + n \log[Q] \tag{2}$$

where n is the number of binding sites, and K_b represents the binding constant. Using eqn (2), the binding parameters for the AgNP/BSA system at different temperatures were determined
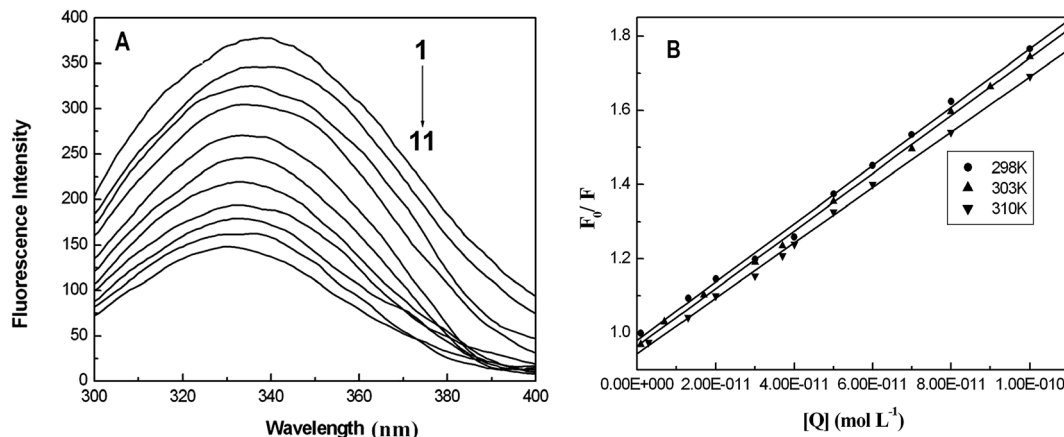
Fig. 1 (A) The fluorescence spectra of BSA in the presence of various concentrations of AgNPs. (B) Stern−Volmer plots for the binding of AgNPs to BSA at different temperatures. The concentration of BSA is 1.0×10^{-6} M, and the concentrations of the AgNPs are (1–11): 0–1.0×10^{-10} M.

Table 1 Stern−Volmer quenching constants for the interaction of AgNPs with BSA at different temperatures

T (K)	K_{SV} (10^9 mol L^{-1})	k_q (10^{17} L mol^{-1} s^{-1})	R^a	SD^b
298	7.724	7.724	0.9917	0.03627
303	7.639	7.639	0.9926	0.03324
310	7.443	7.443	0.9912	0.04164

^{a} R is the correlation coefficient. ^{b} SD is the standard deviation.

and are presented in Table 2. It is seen that K_b decreases as the temperature increases, which is indicative of the formation of a stable AgNP–BSA complex.

In order to reveal energetic changes in the binding of BSA with AgNPs, the thermodynamic parameters of the binding process were further analyzed using the Van't Hoff equation. If the thermodynamic parameters ΔH^0 (change in enthalpy) and ΔS^0 (change in entropy) experience little change over the temperature range, then ΔH^0 and ΔS^0 can be derived from the following equation:[29,32]

$$\ln K_b = -\frac{\Delta H^0}{RT} + \frac{\Delta S^0}{R} \qquad (3)$$

where K_b is the binding constant for the corresponding temperature, T is the experimental temperature and R is the gas constant. ΔG^0 (change in free energy) can be expressed as

$$\Delta G^0 = \Delta H^0 - T\Delta S^0 \qquad (4)$$

Table 2 The thermodynamic parameters of the BSA/AgNP system at different temperatures

T (K)	K_b (10^4 L mol^{-1})	R^a	SD^b	ΔH^0 (kJ mol^{-1})	ΔG^0 (kJ mol^{-1})	ΔS^0 (J mol^{-1})
298	17.14	0.9911	1.0134	−34.63	−39.49	16.31
303	12.65	0.9863	0.8125		−39.57	
310	9.526	0.9868	0.8179		−39.69	

^{a} R is the correlation coefficient. ^{b} SD is the standard deviation.

Fig. S4† illustrates the Van't Hoff plots for the interaction of AgNPs with BSA at different temperatures, and the corresponding thermodynamic parameters (ΔH^0, ΔS^0 and ΔG^0) are also presented in Table 2. The negative value of ΔG^0 indicates the spontaneity of the binding of the AgNPs to BSA. An enthalpy change (ΔH^0) can reflect an increase in the intermolecular bond energies in a binding process, and an entropy change (ΔS) usually reveals a change in the disorder of the system in a binding process. From Table 2, we can find that ΔH^0 is a negative value, while ΔS^0 is a positive value, which demonstrates that the main acting forces during the interaction between the AgNPs and BSA may be hydrogen bonding and hydrophobic interactions.[29] Furthermore, it is seen that the positive value of ΔS^0 and the negative value of ΔH^0 can cooperatively contribute to the negative value of ΔG^0. Therefore, it seems to be implied that the binding of BSA to AgNPs is synergistically driven by enthalpy and entropy.

3.3.   Conformational changes of the protein

In order to explore the effect of the nanoparticles on the microstructure of the protein, synchronous fluorescence, FT-IR and CD spectra were utilized to estimate the conformational changes of BSA induced by the addition of the AgNPs.

Fig. 2A and B show the synchronous fluorescence spectra of BSA with the addition of AgNPs at $\Delta\lambda = 15$ nm and $\Delta\lambda = 60$ nm, respectively. When $\Delta\lambda = 15$ nm (Fig. 2A), it is clear that the fluorescence emission peaks of BSA are blue shifted, which indicates that the interaction of BSA with the AgNPs alters the micro-environmental polarity of the tyrosine (Tyr) residues. Moreover, in this case, the polarity and the hydrophilicity of the Tyr residues are decreased, implying that the Tyr residues were not easily exposed to the aqueous solution. However, when $\Delta\lambda = 60$ nm (Fig. 2B), the emission peaks of the tryptophan (Trp) residues had almost no change, suggesting that the interaction between BSA and the AgNPs did not affect the micro-environment of the Trp residues.[29,32]

FT-IR spectroscopy can be adopted to directly analyze the effect of the AgNPs on the secondary structures of BSA. The FT-
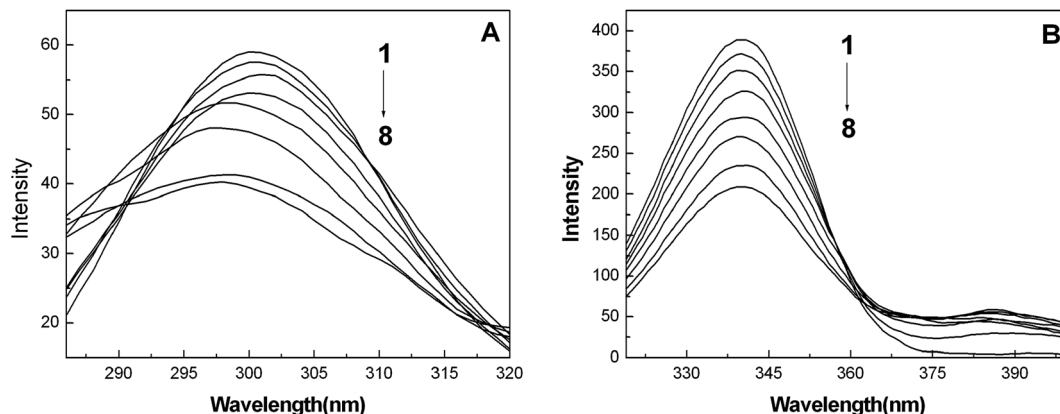
Fig. 2 Synchronous fluorescence spectra of BSA in the absence and presence of AgNPs at pH 7.4. (A) $\Delta\lambda = 15$ nm and (B) $\Delta\lambda = 60$ nm. The concentration of BSA is 1.0×10^{-6} M, and the concentrations of the AgNPs are (1–8): 0–3.7×10^{-11} M.

IR spectra of the protein exhibit a number of amide bands, which represent the different vibrations of the peptide strands. Among the amide bands of the protein, the amide I band (1700–1600 cm^{-1}, mainly C=O stretching) and amide II band (1600–1500 cm^{-1}, C–N stretching coupled with an N–H bending mode) both have relationships with the secondary structure of the protein.[33] However, it is noted that the amide I band is more sensitive to the change in the protein secondary structure than the amide II band.[34] The FT-IR spectra of BSA in the absence and presence of AgNPs in buffer solution were recorded (Fig. S5†). The peak positions of the amide I and II bands were observed at 1653 and 1547 cm^{-1} (BSA, Fig. S5A†), and 1652 and 1546 cm^{-1} (BSA/AgNP, Fig. S5B†) together with changes in the shape and intensity of the peaks upon the addition of AgNPs to BSA. These results indicate that the AgNPs interact with both the C=O and C–N groups in the protein polypeptides, resulting in a rearrangement of the polypeptide carbonyl hydrogen-bonding network. So, these observations confirm that the α-helical content of BSA may decrease with the addition of AgNPs.

To further evaluate the conformational changes of the protein, the binding of the AgNPs to BSA was also studied using CD spectroscopy. CD is a sensitive technique to monitor the conformational changes of proteins. The CD spectra of BSA in the absence and presence of AgNPs are shown in Fig. 3. It is seen that the CD spectra of BSA exhibit two negative bands at 208 and 222 nm, which are characteristic of a typical α-helix structure of a protein. The binding of the AgNPs to BSA leads to a decrease in the negative ellipticity at all the wavelengths of the far UV CD without any obvious shift of the peaks, which clearly indicates a change in the protein secondary structure (a decrease in the α-helix content of BSA).[35] The percentage of α-helix content can be calculated using the following equation:[36]

$$\alpha\text{-Helix}(\%) = \left[\frac{-\text{MRE208} - 4000}{33\,000 - 4000}\right] \times 100 \quad (5)$$

where MRE$_{208}$ is the observed mean residue ellipticity (MRE) value at 208 nm, 4000 is the MRE of the β-form and random coil conformation cross at 208 nm, and 33 000 is the MRE value of the pure α-helix at 208 nm.

$$\text{MRE}_{208} = \frac{\text{observed CD(mdeg)}}{C_p nl \times 10} \quad (6)$$

where C_p is the molar concentration of the protein (BSA), n is the number of amino acid residues (583 for BSA) and l is the path length (1.0 cm). The α-helix content of the protein was determined from eqn (5) and (6). In our case, it can be calculated that the α-helix content of the native BSA is 56.21%, while the α-helix content of BSA decreases to 54.67%, 53.11% and 49.85% with the addition of AgNPs at concentrations of 2.0×10^{-11} M, 6.0×10^{-11} M and 2.0×10^{-10} M, respectively. Therefore, the observations of the CD spectra are confirmed to be in accordance with the results of the FT-IR experiment. The secondary structure content of proteins is closely related to their biological activities, so the above results imply a loss of the biological activity of BSA. This result suggests the occurrence of a conformational change at the secondary structural level with the binding of AgNPs to BSA.[37]
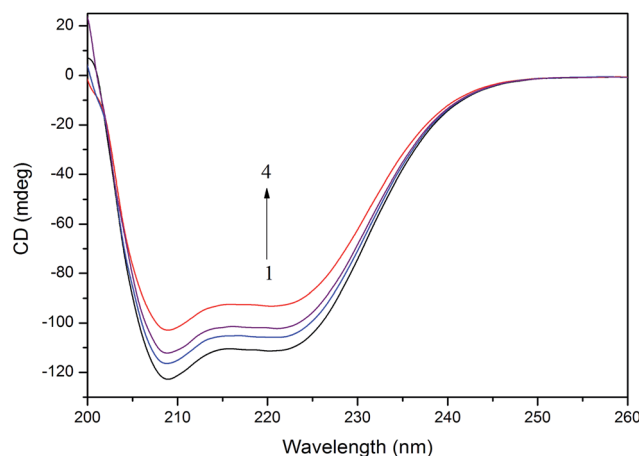

Fig. 3 CD spectra of BSA in the absence and presence of AgNPs. The concentration of BSA is 1×10^{-6} M, and the concentrations of AgNPs are (1–4): 0, 2.0×10^{-11} M, 6.0×10^{-11} M, and 2.0×10^{-10} M, respectively.

3.4. Kinetics of adsorption process

3.4.1. Hysteresis effect for the interaction of AgNPs with BSA.
If we presume that the interaction of AgNPs with BSA is a monolayer adsorption process, the hysteresis effect can be explored by studying the changes in the absorption of AgNPs with an increasing concentration of BSA. From Fig. 4A, we can see that the absorbance peak of the AgNPs at 416 nm seems to be slightly red shifted then increasingly blue shifted, while the absorption intensity decreased gradually with the addition of BSA. This indicates that the surfaces of the AgNPs were coated with BSA molecules, and the adsorption was gradually enhanced with an increase in the concentration of BSA. Additionally, it is shown that the absorption intensity of the AgNPs tends to stabilise with the addition of BSA (Fig. 4B), which implies that the binding of BSA with AgNPs reaches saturation. According to the above results, it can be concluded that the interaction of AgNPs with BSA possesses an obvious hysteresis effect.

3.4.2. Kinetics model.
Adsorption kinetics are important for adsorption studies because they can predict the rate at which BSA is adsorbed on the surface of the AgNPs from the aqueous solution and provide valuable information for understanding the mechanism of the adsorption reactions.[38] The adsorption kinetics for the binding of BSA on the surface of the AgNPs were investigated with an initial concentration of BSA of 250 mg L^{-1}. The concentration of AgNPs was adjusted to 20 mg L^{-1}. At various time intervals, the suspension was centrifuged and the concentration of BSA remaining in the supernatant was determined. The amount of adsorption (q_t) at time t was calculated using the following equation:[39–41]

$$q_e = \frac{(C_0 - C_t)V}{W} \qquad (7)$$

where C_0 and C_t (mg L^{-1}) are the concentration of BSA initially and at time t, respectively, V is the volume of the solution (L) and W is the mass of AgNPs used.

The binding kinetics of BSA on the surface of the AgNPs were estimated using two fundamental kinetic models (pseudo-first-order and pseudo-second-order). The linear expression of the pseudo-first-order model can be written as:[40]

$$\log(q_e - q_t) = \log q_e - \frac{k_1}{2.303}t \qquad (8)$$

In this equation, q_e and q_t represent the amount of adsorbed BSA on the surface of the AgNPs in an equilibrium state and at reaction time t, respectively. k_1 is the equilibrium rate constant of pseudo-first-order adsorption. The values of the correlation coefficients (R^2) are adopted to evaluate the dependence of the linear relationship. According to the linear form of eqn (8), $\log(q_e - q_t)$ *versus* t was fitted to determine k_1 and q_e (Fig. 5A). It is obvious that the R^2 values obtained here are relatively small. Additionally, the pseudo-first-order rate constant k_1 and q_e determined from this model indicate that the experimental q_e value is not in accordance with the calculated value. Therefore, it is shown that the kinetic behavior of the binding of AgNPs to BSA seems to not match the pseudo-first-order kinetic model.

The linear form of the pseudo-second-order equation can be written as:[40]

$$\frac{t}{q_t} = \frac{1}{k_2(q_e)^2} + \frac{t}{q_e} \qquad (9)$$

where k_2 is the equilibrium rate constant of pseudo-second-order adsorption. The values of the second order rate constant k_2 and q_e were derived from the fitted linear plot (Fig. 5B). We can see that the R^2 value is greater than 0.999, and the theoretical q_e value agrees well with the experimental q_e value. From the combination of these observations, we can confirm that the adsorption kinetics of the binding of AgNPs to BSA tends to follow the pseudo-second-order kinetic model.

Adsorption isotherms are a significant approach to study the adsorption capacity of ligands on the surface of nanoparticles. Along this line, Freundlich and Langmuir isotherms have usually been used to describe the adsorption process of NPs with biological systems.[39,41] The adsorption parameters of the BSA/AgNP system were fitted according to the linear forms of
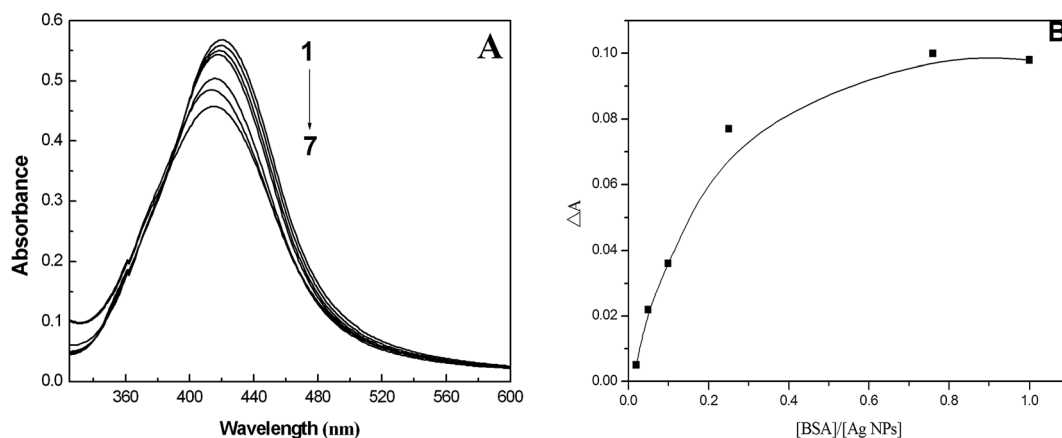

Fig. 4 (A) The surface plasmon resonance absorption of different concentrations of BSA with AgNPs. [AgNPs] = 1.0 × 10^{-4} M, 1–7: [BSA]/[AgNPs] = 0, 1 : 50, 1 : 40, 1 : 30, 1 : 20, 1 : 10, and 1 : 1; (B) the relationship between the change in the absorption intensity (ΔA) and [BSA]/[AgNPs].
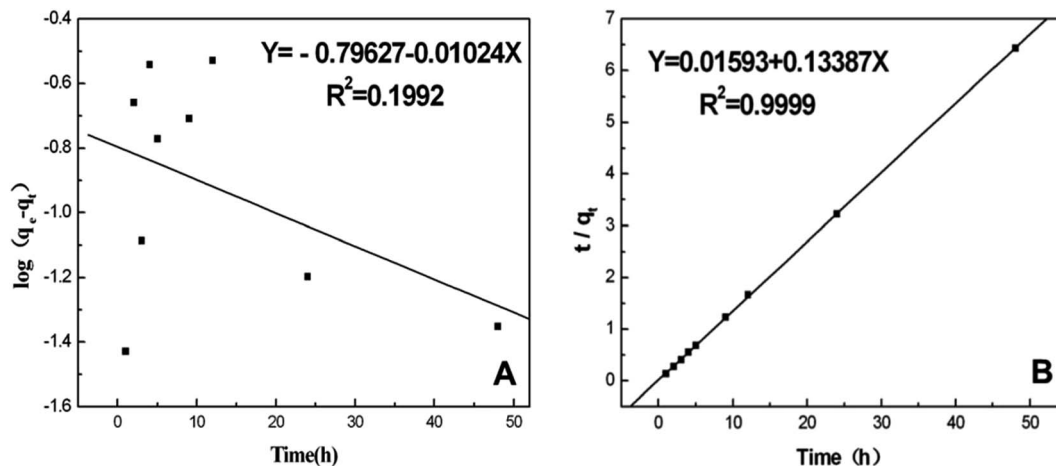
Fig. 5 (A) The pseudo-first-order kinetics plotted as a function of $\log(q_e - q_t)$ *versus* time (t) and (B) the pseudo-second-order kinetics plotted as a function of t/q_t *versus* time (t).

both the Freundlich and Langmuir adsorption isotherms to seek the optimal isothermal adsorption model. Fig. 6 shows the adsorption isotherms of BSA on the surface of AgNPs at room temperature. Here BSA and the AgNPs are, respectively, the adsorbate and the adsorbent.

The multilayer adsorption on a particle surface can be evaluated using the Freundlich adsorption isotherm model. The Freundlich equation is an empirical equation and can be expressed as follows:

$$q_e = K_F C_e^{1/n} \qquad (10)$$

where C_e is the mass concentration of BSA in the supernatant (mg L^{-1}), q_e is the amount of BSA (mg) adsorbed per mg of AgNPs in equilibrium, and K_F is the Freundlich constant. A linear form of the Freundlich expression can be obtained by taking the logarithm of eqn (10):[40]

$$\log q_e = \frac{1}{n}\log C_e + \log K_F \qquad (11)$$

The plot of $\log q_e$ *versus* $\log C_e$ allows the constant K_F and the exponent $1/n$ to be determined (Fig. 6A). The Freundlich isotherm describes the multilayer adsorption and is not restricted to the formation of a monolayer. The Freundlich equation predicts that the BSA concentration on the adsorbent will increase so long as there is an increase in BSA concentration in the current environment. The Freundlich isotherm constants were also manually calculated. It is obvious that the experimental data fitted well to the Freundlich model, suggesting the multilayer adsorption of BSA on the surface of the AgNPs. The high R^2 value (linear regression coefficient) indicates that the Freundlich model predicts the adsorption behavior of BSA on AgNPs well.

The Langmuir isothermal adsorption model postulates that once an adsorbate molecule occupies a site on the adsorbent, this site can not further adsorb any other adsorbate molecules. The Langmuir isothermal adsorption model can be formulated as the following equation:
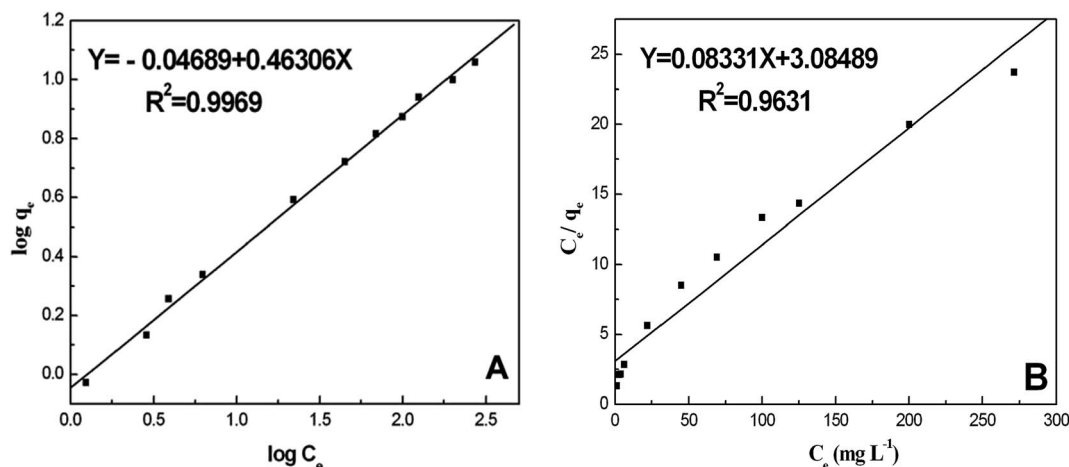

Fig. 6 (A) Freundlich isothermal adsorption of BSA on the surface of the AgNPs; (B) Langmuir isothermal adsorption of BSA on the surface of AgNPs.

$$q_e = \frac{q_m K_a C_e}{1 + K_a C_e} \qquad (12)$$

where C_e is the mass concentration of BSA in the supernatant (mg L^{-1}), q_e is the amount of BSA (mg) adsorbed per mg of AgNPs, and q_m is the maximum adsorption amount of BSA on the surface of the AgNPs for a monolayer. K_a is the adsorption constant (L mg^{-1}), which shows the binding affinity of BSA on the surface of the AgNPs.

Eqn (12) may be rewritten in the following linear form:[40]

$$\frac{C_e}{q_e} = \frac{C_e}{q_m} + \frac{1}{K_a q_m} \qquad (13)$$

In this equation, the values of q_m and K_a can be calculated using a linear plot of C_e/q_e versus C_e (Fig. 6B). The Langmuir isotherm constants were also manually calculated by solving the simultaneous equations. Obviously, the large variations between the graphical solution and the analytical solutions indicate that the experimental data do not fit well to the Langmuir model. The relatively low R^2 value (linear regression coefficient) indicates that the Langmuir model does not correspond well with the adsorption behavior of BSA on AgNPs.

4. Conclusions

In this study, the interactions between the protein BSA and AgNPs were investigated using multiple spectroscopic techniques. It is shown that BSA interacts with AgNPs to form a stable BSA-AgNP complex. At the same time, the results implied that the interaction of AgNPs with BSA may be a static quenching process, and the process is spontaneous with the major acting forces being hydrogen bonding and hydrophobic interactions. We also found evidence of significant conformational changes in the proteins. Additionally, the adsorption of BSA on the AgNP surfaces tends to follow pseudo-second-order kinetics with an obvious hysteresis effect. Notably, we found that the experimental data fitted well with the Freundlich isotherm model, which indicates the multilayer adsorption. The binding behaviors and kinetics of AgNPs with proteins are important aspects in realizing the toxicity and safety of AgNPs in biological and medical fields. With these findings, in the future, we can also focus on various factors such as the size, charge and surface composition of NPs, facilitating the evaluation of the effect of various factors on the binding properties of NP-protein systems, which has great significance for the safe application of NPs in biological systems.

Acknowledgements

References

1 W. Wu, M. Wu, Z. Sun, G. Li, Y. Ma, X. Liu, X. Wang and X. Chen, Morphology controllable synthesis of silver nanoparticles: Optical properties study and SERS application, *J. Alloys Compd.*, 2013, **579**, 117–123.

2 M. Ahamed, M. S. Alsalhi and M. K. J. Siddiqui, Silver nanoparticle applications and human health, *Clin. Chim. Acta*, 2010, **411**, 1841–1848.

3 M. Rai, A. Yadav and A. Gade, Silver nanoparticles as a new generation of antimicrobials, *Biotechnol. Adv.*, 2009, **27**, 76–83.

4 V. K. Sharma, R. A. Yngard and Y. Lin, Silver nanoparticles: green synthesis and their antimicrobial activities, *Adv. Colloid Interface Sci.*, 2009, **145**, 83–96.

5 L. Wei, J. Lu, H. Xu, A. Patel, Z. S. Chen and G. Chen, Silver nanoparticles: synthesis, properties, and therapeutic applications, *Drug Discovery Today*, 2015, **20**, 595–601.

6 A. Ravindran, P. Chandran and S. S. Khan, Biofunctionalized silver nanoparticles: advances and prospects, *Colloids Surf., B*, 2013, **105**, 342–352.

7 A. Gebregeorgis, C. Bhan, O. Wilson and D. Raghavan, Characterization of silver/bovine serum albumin (Ag/BSA) nanoparticles structure: morphological, compositional, and interaction studies, *J. Colloid Interface Sci.*, 2013, **389**, 31–41.

8 A. Sasidharan, J. E. Riviere and N. A. Monteiro-Riviere, Gold and silver nanoparticle interactions with human proteins: impact and implications in biocorona formation, *J. Mater. Chem. B*, 2013, **3**, 2075–2082.

9 Q. Wang, M. Lim, X. Liu, Z. Wang and K. L. Chen, Influence of solution chemistry and soft protein coronas on the interactions of silver nanoparticles with model biological membranes, *Environ. Sci. Technol.*, 2016, **50**, 2301–2309.

10 J. T. Tai, C. S. Lai, H. C. Ho, Y. S. Yeh, H. F. Wang, R. M. Ho and D. H. Tsai, Protein-silver nanoparticle interactions to colloidal stability in acidic environments, *Langmuir*, 2014, **30**, 12755–12764.

11 R. Eigenheer, E. R. Castellanos, M. Y. Nakamoto, K. T. Gerner, A. M. Lampe and K. E. Wheeler, Silver nanoparticle protein corona composition compared across engineered particle properties and environmentally relevant reaction conditions, *Environ. Sci.: Nano*, 2014, **1**, 238–247.

12 V. K. Sharma, K. M. Siskova, R. Zboril and J. L. Gardea-Torresdey, Organic-coated silver nanoparticles in biological and environmental conditions: fate, stability and toxicity, *Adv. Colloid Interface Sci.*, 2014, **204**, 15–34.

13 M. Sajid Ali, H. A. Al-Lohedan, M. Z. A. Rafiquee, A. M. Atta and A. O. Ezzat, Spectroscopic studies on the interaction between novel polyvinylthiol-functionalized silver nanoparticles with lysozyme, *Spectrochim. Acta, Part A*, 2015, **135**, 147–152.

14 K. B. Ayaz Ahmed, A. S. Mohammed and V. Anbazhagan, Interaction of sugar stabilized silver nanoparticles with the T-antigen specific lectin, jacalin from *Artocarpus integrifolia*, *Spectrochim. Acta, Part A*, 2015, **145**, 110–116.

15 M. Dell'Aglio, V. Mangini, G. Valenza, O. De Pascale, A. De Stradis, G. Natile, F. Arnesano and A. De Giacomo, Silver and gold nanoparticles produced by pulsed laser ablation in liquid to investigate their interaction with ubiquitin, *Appl. Surf. Sci.*, 2016, **374**, 297–304.

16 K. Siriwardana, A. Wang, M. Gadogbe, W. E. Collier, N. C. Fitzkee and D. Zhang, Studying the effects of cysteine residues on protein interactions with silver nanoparticles, *J. Phys. Chem. C*, 2015, **119**, 2910–2916.

17 Y. Wang and Y. Ni, New insight into protein-nanomaterial interactions with UV-visible spectroscopy and chemometrics: human serum albumin and silver nanoparticles, *Analyst*, 2014, **139**, 416–424.

18 L. K. Ono, S. R. Raga, S. H. Wang, Y. C. Kato and Y. B. Qi, Temperature-dependent hysteresis effects in perovskite-based solar cells, *J. Mater. Chem. A*, 2015, **3**, 9074–9080.

19 B. Wang, S. A. Seabrook, P. Nedumpully-Govindan, P. Chen, H. Yin, L. Waddington, V. Chandana Epa, D. A. Winkler, J. K. Kirby, F. Ding and P. C. Ke, Thermostability and reversibility of silver nanoparticle-protein binding, *Phys. Chem. Chem. Phys.*, 2015, **17**, 1728–1739.

20 V. P. Brahmkhatri, K. Chandra, A. Dubey and H. S. Atreya, An ultrastable conjugate of silver nanoparticles and protein formed through weak interactions, *Nanoscale*, 2015, **7**, 12921–12931.

21 S. Zhang, Y. Moustafa and Q. Huo, Different interaction modes of biomolecules with citrate-capped gold nanoparticles, *ACS Appl. Mater. Interfaces*, 2014, **6**, 21184–21192.

22 A. Wang, K. Vangala, T. Vo, D. Zhang and N. C. Fitzkee, A three-step model for protein–gold nanoparticle adsorption, *J. Phys. Chem. C*, 2014, **118**, 8134–8142.

23 R. Huang, R. P. Carney, K. Ikuma, F. Stellacci and B. L. Lau, Effects of surface compositional and structural heterogeneity on nanoparticle-protein interactions: different protein configurations, *ACS Nano*, 2014, **8**, 5402–5412.

24 D. Docter, D. Westmeier, M. Markiewicz, S. Stolte, S. K. Knauer and R. H. Stauber, The nanoparticle biomolecule corona: lessons learned-challenge accepted, *Chem. Soc. Rev.*, 2015, **44**, 6094–6121.

25 M. A. Dobrovolskaia, B. W. Neun, S. Man, X. Ye, M. Hansen, A. K. Patri, R. M. Crist and S. E. Mcneil, Protein corona composition does not accurately predict hematocompatibility of colloidal gold nanoparticles, *Nanomedicine*, 2014, **10**, 1453–1463.

26 C. Munro, W. Smith, M. Garner, J. Clarkson and P. White, Characterization of the surface of a citrate-reduced colloid optimized for use as a substrate for surface-enhanced resonance Raman scattering, *Langmuir*, 1995, **11**, 3712–3720.

27 D. G. Thompson, A. Enright, K. Faulds, W. E. Smith and D. Graham, Ultrasensitive DNA detection using oligonucleotide-silver nanoparticle conjugates, *Anal. Chem.*, 2008, **80**, 2805–2810.

28 C. Krishnaraj, E. G. Jagan, S. Rajasekar, P. Selvakumar, P. T. Kalaichelvan and N. Mohan, Synthesis of silver nanoparticles using *Acalypha indica* leaf extracts and its antibacterial activity against water borne pathogens, *Colloids Surf., B*, 2010, **76**, 50–56.

29 G. K. Wang, X. B. Liu, C. L. Yan, G. Y. Bai and Y. Lu, Probing the binding of trypsin to glutathione-stabilized gold nanoparticles in aqueous solution, *Colloids Surf., B*, 2015, **135**, 261–266.

30 J. Mariam, P. M. Dongre and D. C. Kothari, Study of interaction of silver nanoparticles with bovine serum albumin using fluorescence spectroscopy, *J. Fluoresc.*, 2011, **21**, 2193–2199.

31 Q. Yang, J. Liang and H. Han, Probing the interaction of magnetic iron oxide nanoparticles with bovine serum albumin by spectroscopic techniques, *J. Phys. Chem. B*, 2009, **113**, 10454–10458.

32 G. K. Wang, Y. Chen, C. L. Yan and Y. Lu, Study on the interaction between gold nanoparticles and papain by spectroscopic methods, *J. Lumin.*, 2015, **157**, 229–234.

33 J. Tian, J. Liu, W. He, Z. Hu, X. Yao and X. Chen, Probing the binding of scutellarin to human serum albumin by circular dichroism, fluorescence spectroscopy, FTIR, and molecular modeling method, *Biomacromolecules*, 2004, **5**, 1956–1961.

34 K. Rahmelow and W. Hübner, Secondary structure determination of proteins in aqueous solution by infrared spectroscopy: a comparison of multivariate data analysis methods, *Anal. Biochem.*, 1996, **241**, 5–13.

35 X. L. Han, F. F. Tian, Y. S. Ge, F. L. Jiang, L. Lai, D. W. Li, Q. L. Yu, J. Wang, C. Lin and Y. Liu, Spectroscopic, structural and thermodynamic properties of chlorpyrifos bound to serum albumin: a comparative study between BSA and HSA, *J. Photochem. Photobiol., B*, 2012, **109**, 1–11.

36 A. Bhogale, N. Patel, J. Mariam, P. M. Dongre, A. Miotello and D. C. Kothari, Comprehensive studies on the interaction of copper nanoparticles with bovine serum albumin using various spectroscopies, *Colloids Surf., B*, 2014, **113**, 276–284.

37 S. Cao, B. Liu, Z. Li and B. Chong, A fluorescence spectroscopic study of the interaction between glipizide and bovine serum albumin and its analytical application, *J. Lumin.*, 2014, **145**, 94–99.

38 S. S. Khan, P. Srivatsan, N. Vaishnavi, A. Mukherjee and N. Chandrasekaran, Interaction of silver nanoparticles (SNPs) with bacterial extracellular proteins (ECPs) and its adsorption isotherms and kinetics, *J. Hazard. Mater.*, 2011, **192**, 299–306.

39 N. Hoda, E. Bayram and E. Ayranci, Kinetic and equilibrium studies on the removal of acid dyes from aqueous solutions by adsorption onto activated carbon cloth, *J. Hazard. Mater.*, 2006, **137**, 344–351.

40 S. S. Khan, A. Mukherjee and N. Chandrasekaran, Interaction of colloidal silver nanoparticles (SNPs) with exopolysaccharides (EPS) and its adsorption isotherms and kinetics, *Colloids Surf., A*, 2011, **381**, 99–105.

41 S. S. Khan, A. Mukherjee and N. Chandrasekaran, Adsorptive removal of silver nanoparticles (SNPs) from aqueous solution by *Aeromonas punctata* and its adsorption isotherm and kinetics, *Colloids Surf., B*, 2012, **92**, 156–160.